ACS chemical biology

Articles

pubs.acs.org/acschemicalbiology

Electrostatic Effect of the Ribosomal Surface on Nascent Polypeptide Dynamics

Anders M. Knight,[†,§] Peter H. Culviner,[†,§,∥] Neşe Kurt-Yilmaz,[†,⊥] Taisong Zou,[‡] S. Banu Ozkan,[‡] and Silvia Cavagnero*[,†]

[†]Department of Chemistry, University of Wisconsin-Madison, 1101 University Avenue, Madison, Wisconsin 53706, United States

[‡]Department of Physics, Center for Biological Physics, Arizona State University, Tempe, Arizona 85287, United States

Supporting Information

ABSTRACT: The crucial molecular events accompanying protein folding in the cell are still largely unexplored. As nascent polypeptides emerge from the ribosomal exit tunnel, they come in close proximity with the highly negatively charged ribosomal surface. How is the nascent polypeptide influenced by the ribosomal surface? We address this question via the intrinsically disordered protein PIR and a number of its variably charged mutants. Two different populations are identified: one is highly spatially biased, and the other is highly dynamic. The more negatively charged nascent polypeptides emerging from the ribosome are richer in the extremely dynamic population. Hence, nascent proteins with a net negative charge are less likely to interact with the ribosome. Surprisingly, the amplitude of the local motions of the highly dynamic population is much wider than that of disordered polypeptides under physiological conditions, implying that proximity to the ribosomal surface enhances the molecular flexibility of a subpopulation of the nascent protein, much like a denaturing agent would. This effect could be important for a proper structural channeling of the nascent protein and the prevention of cotranslational kinetic trapping. Interestingly, a significant population of the highly spatially biased nascent chain, probably interacting extensively with the ribosome, is present even for very negatively charged nascent proteins. This "sticking" effect likely serves to protect nascent proteins (e.g., from cotranslational aggregation). In all, our results highlight the influence of the ribosome in nascent protein dynamics and show that the ribosome's function in protein biogenesis extends well beyond catalysis of peptide bond formation.

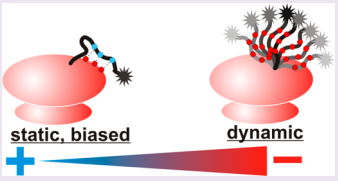

Despite its prominent role in biology, we know very little about protein folding in the cell. Recent investigations provided evidence for the partial folding of nascent proteins even before biosynthesis is complete and fueled hypotheses on the role of the different translation components in this process.[1−4] Information is still sparse, and the role of the ribosome, i.e., the central element of translation, in cotranslational protein folding is still largely unexplored.

Newly synthesized polypeptides travel through the exit tunnel in the large subunit of the ribosome (Figure 1a) before emerging into the cellular milieu. During their journey through the tunnel, nascent polypeptides experience very narrow local motions[5] and assume either α-helical structure, a more extended conformation,[6,7] or a combination of the two. Larger structural motifs with tertiary contacts can fit in the last ∼20% of the tunnel as the protein emerges from the ribosome.[8] While some structural information is available on how the ribosomal tunnel affects polypeptide conformational sampling, virtually nothing is known on the role of the ribosomal outer surface in nascent protein folding.

The ribosomal surface has a highly negative electrostatic potential[9,10] arising primarily from the phosphodiester backbone of the rRNA (Figure 1b). We know that the outer surface of the ribosome imposes severe constraints on the amplitude of the local motions of compact domains emerging out of its surface[5] and slows down folding/unfolding transitions.[11] Computations not taking electrostatics into account predicted that entropic effects at the ribosome surface destabilize nascent proteins structure.[12] On the other hand, nothing is known about the role of nascent protein's net charge near the ribosomal surface.

The net charge of a protein is one of its most fundamental physical properties and plays a seminal role in biology, influencing stability, complex formation, and ligand binding.[13−15] Together with hydrophobicity, net charge and specific charge location play a key role in protein foldability and affect the interplay between protein folding and aggregation.[16−19]

An important unanswered question is whether the net charge of a nascent polypeptide emerging out of the ribosome influences its conformation and dynamics in proximity of the negatively charged ribosomal surface. We explore this topic here by analyzing nascent chains derived from the phosphorylated insulin receptor interaction region of Grb14 from rat, known as PIR.[20] PIR is an intrinsically disordered protein (i.e., an IDP) devoid of interaction with cotranslationally active chaperones[5] and lacking the ability to fold in the absence of its biological counterpart.[20,21] Hence, the PIR sequence enables investigating nascent chain dynamics in the absence of any complications arising from driving forces for folding. We studied the role of electrostatics by mutating the PIR sequence

Received: January 14, 2013
Accepted: March 21, 2013
Published: March 21, 2013

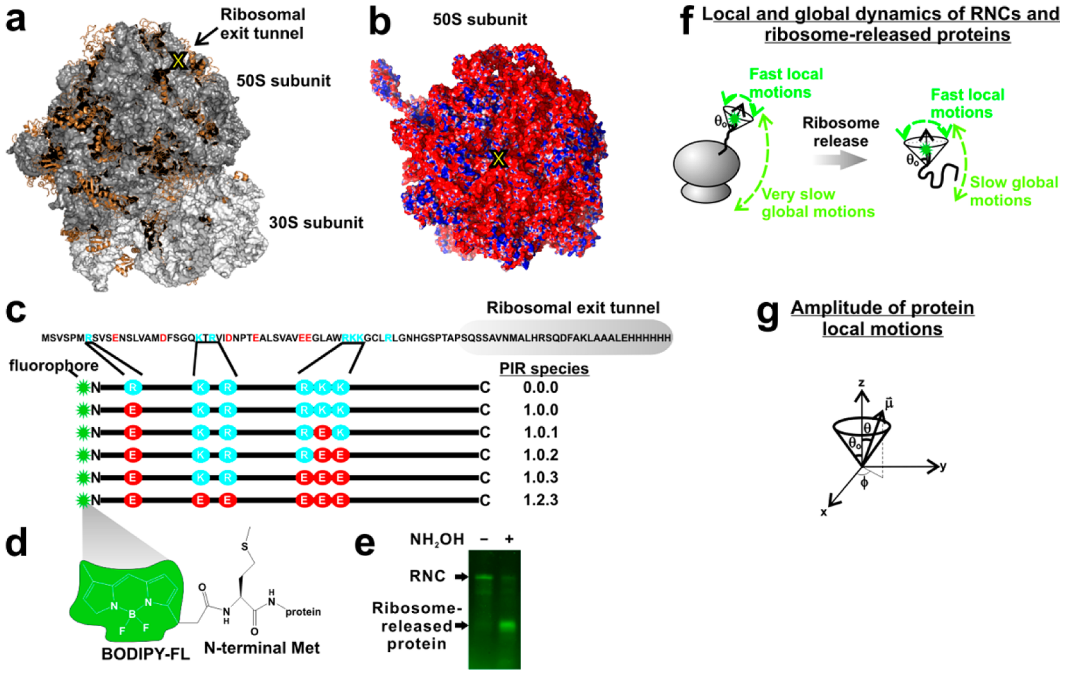

Figure 1. General features of the bacterial ribosome and PIR nascent chains. (a) Crystal structure of the *E. coli* ribosome[50] (PDB IDs: 2AVY and 2AW4). The rRNA is shown in gray (23S and 5S RNAs: dark gray; 16S RNA: light gray), and the ribosomal proteins are displayed in brown. The tunnel exit in the 50S subunit is denoted by a yellow x. (b) Surface electrostatic potential map of the *E. coli* ribosome 50S subunit in proximity of the exit tunnel. The surface is colored according to the electrostatic potential from −5 kT/e (red) to +5 kT/e (blue), with white denoting 0 kT/e. (c) Schematic illustration of the PIR sequence with acidic and basic residues emerging out of the tunnel shown in red and blue, respectively. The portion of the chain expected to be buried within the ribosomal tunnel is shaded in gray. The wild-type and mutants are defined as shown in this panel and in the Methods section. (d) Schematic structure of the nascent chain N terminus bearing the Bodipy-FL fluorophore. (e) Fluorescence-detected SDS-PAGE analysis of ribosome-bound and ribosome-released wild-type PIR. (f) Cartoon illustrating the local (dark green, involving the N-terminal residues) and global (light green, involving the whole molecule) motions of ribosome-bound and ribosome-released nascent proteins that are not significantly structured while bound to the ribosome. (g) Geometrical definition of the cone semi-angle θ_0 describing the amplitude of the local protein dynamics. The vector μ defines the emission dipole moment of the fluorophore experiencing the local motions, in a macromolecule-fixed reference frame with a normal along the z axis.

at selected sites so that its net charge undergoes variations in both sign (from positive to negative) and magnitude. Nascent chain flexibility was probed by studying the motions of nascent PIR's N-terminal region by dynamic fluorescence depolarization in the frequency domain.

We found evidence for two nascent chain populations, one highly spatially biased and one highly dynamic. The former prevails in the case of wild-type nascent PIR, whose sequence emerging out of the ribosomal tunnel has a net positive charge. The highly dynamic species experiences unusually wide-amplitude local motions. The population of this species increases when the net charge of the nascent chain is strongly negative, consistent with fewer interactions with the negatively charged ribosomal surface. Remarkably, regardless of the net charge of the nascent protein, a significant population of spatially biased nascent chain persists. Given that this spatially biased population is devoid of any detectable tumbling on the nanosecond time scale,[22] it likely undergoes extensive interactions with the ribosome.

RESULTS AND DISCUSSION

Nascent Protein Labeling and Experimental Design. To test whether the nascent protein's net charge has an effect on its conformation and dynamics, we replaced positively charged residues in the N-terminal region emerging out of the ribosome with negatively charged Glu. The resulting PIR variants bear a variable net charge spanning from +1.1 (wild-type) to −10.9 (1.2.3 mutant) for all of the residues outside the ribosomal tunnel (Figure 1c). We assumed 30 residues to be buried inside the tunnel.[23,24] The N terminus of each nascent chain was specifically labeled with a Bodipy fluorophore (Bodipy FL) via Bodipy-Met-tRNA^{fMet} (Figure 1d), and the nascent protein length homogeneity was assessed via SDS-PAGE (Figure 1e). The site-specific fluorophore label serves as a powerful reporter of the nascent protein's conformational properties. First, the fluorophore lifetime (Figures 2, 3a and b), steady-state emission spectra and spectral shifts (Figure 3c−e) yield valuable information on the environment and degree of polarity around the PIR's N terminus. Second, analysis of the time-resolved fluorescence depolarization decay of ribosome-bound nascent chains (RNCs)[5,22,25] enables discriminating the local motions of the nascent chain from the global dynamics of the entire ribosomal complex (Figures 1f and 2). This experiment proved to be crucial to assess the population of different classes of RNCs. It was also essential to estimate the amplitude of the local motions of PIR's N terminus via measurement of the cone semi-angle θ_0 (Figure 1g).[26] Importantly, assessing the properties of a nascent protein emerging out of the ribosomal tunnel would have been practically impossible or difficult to interpret via alternative biochemical approaches such as limited proteolysis or cross-linking.

The Ribosomal Surface Environment Is Very Different from Bulk Solution. The lifetime of the Bodipy N-terminal

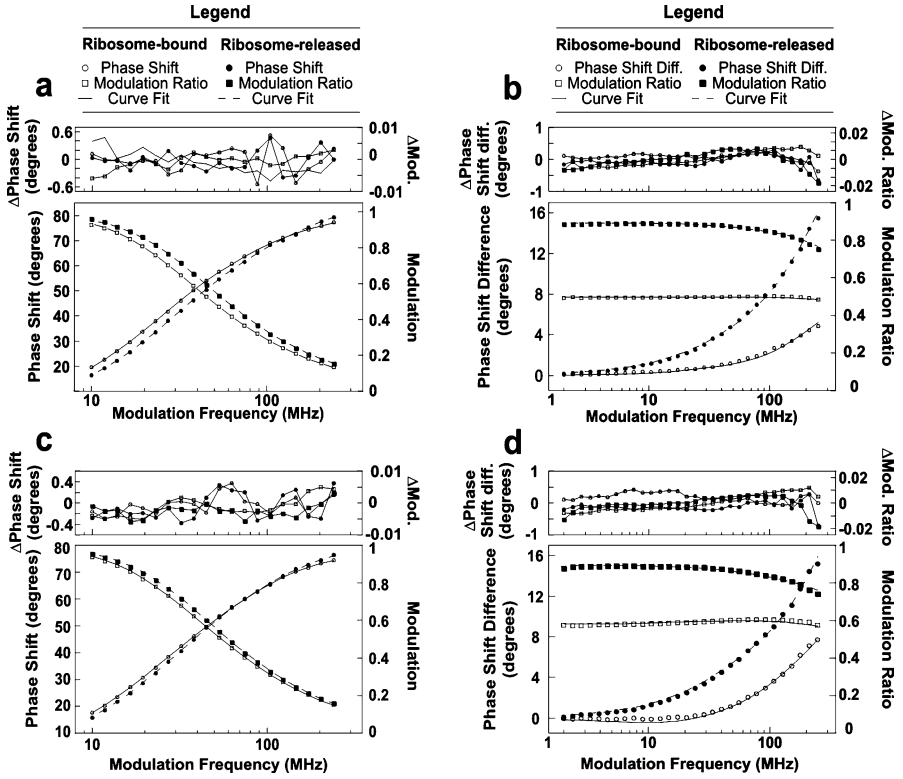

Figure 2. Representative frequency-domain fluorescence lifetime and anisotropy decay data for ribosome-bound and ribosome-released wild-type PIR ($PIR_{0.0.0}$). (a,c) Lifetime data with three-exponential fits and residuals for $PIR_{0.0.0}$ and $PIR_{1.2.3}$, respectively. (b,d) Fluorescence anisotropy decays data with curve fits and residuals for $PIR_{0.0.0}$ and $PIR_{1.2.3}$, respectively.

tag is a powerful sensor of the differences in the ribosome-bound and ribosome-released nascent protein environments. Supplementary Table 1 shows that the protein-linked fluorophore always displays two lifetimes (4−5.5 ns, 1.5−2.5 ns), suggesting the presence of two local conformers in the proximity of the PIR's N-terminus. Individual values of the average fluorescence lifetime are clear indicators of proximity to the ribosome, given that the average lifetime of the nascent chain decreases significantly upon release from the ribosome (Figure 3a). This result is consistent with the presence of additional nonradiative processes in bulk solution, possibly due to the quenching action of Cl^- in the resuspension buffer (Supplementary Figure 1b). Proximity of the nascent protein to the ribosome exerts protection from these processes. This protection may be due to a layer of predominantly positively charged counterions known to be present near the ribosomal surface,[27] which are expected to exclude the negative charged chloride ion, precluding its quenching action. Interestingly, the positively charged wild-type nascent PIR is more strongly protected than the highly negatively charged variants, consistent with a weaker repulsion from the ribosomal surface. Variations in the large and small lifetimes upon release from the ribosome are internally consistent (Supplementary Figure 1a), showing that both lifetimes are comparably good indicators of proximity to the surface.

The phasor plot[28−30] offers a complementary, curve-fitting-independent view of the overall lifetime changes that occur in nascent PIR upon release from the ribosome (Figure 3b). The position of all of the PIR data points inside the universal circle is consistent with the presence of more than one lifetime for all of the protein-linked fluorophores.[28,29,31] This scenario is in contrast with the phasor plot of free Bodipy FL, which lies on the universal circle due to its single-exponential intensity decay. The phasor plot points to progressive lifetime changes for the variably charged RNCs with clockwise displacements (leading to higher G and lower S) as nascent chain net charge increases, suggesting a greater contribution of shorter lifetime components. Conversely, the ribosome-released nascent chains are all clustered despite their different net charge. Hence, the phasor plot shows that variations in nascent chain net charge have a greater impact on RNCs than on released chains, suggesting a ribosomal effect.

Fluorescence emission Stokes shifts (Figure 3c, d and e) offer additional information on the properties of the nascent protein. The red shift of the RNCs relative to ribosome-released PIR indicates a more polar environment,[32] consistent with the high concentration of ions and counterions near the ribosomal surface.

Negatively Charged RNCs Are More Dynamic than Positively Charged RNCs. The most important insights on the effect of electrostatics on nascent chain dynamics are provided by the anisotropy decay data (Figure 4, Supplementary Table 2). The dynamic fluorescence depolarization data for PIR and its variants (Figure 2) display a characteristic increase of modulation ratio at high frequencies. After systematic data fitting with a variety of increasingly more complex models, the simplest scenario that was necessary and sufficient to adequately fit the experimental data is the associative model[33−35] shown in Supplementary Figure 2. This model demands the presence of two nascent chain populations, each associated with one of the fluorescence lifetimes. Each of the two populations displays distinct dynamics. The first population is highly spatially biased and has highly restricted motions (order parameter $0.6 < S < 0.8$),

dx.doi.org/10.1021/cb400030n | ACS Chem. Biol. 2013, 8, 1195−1204

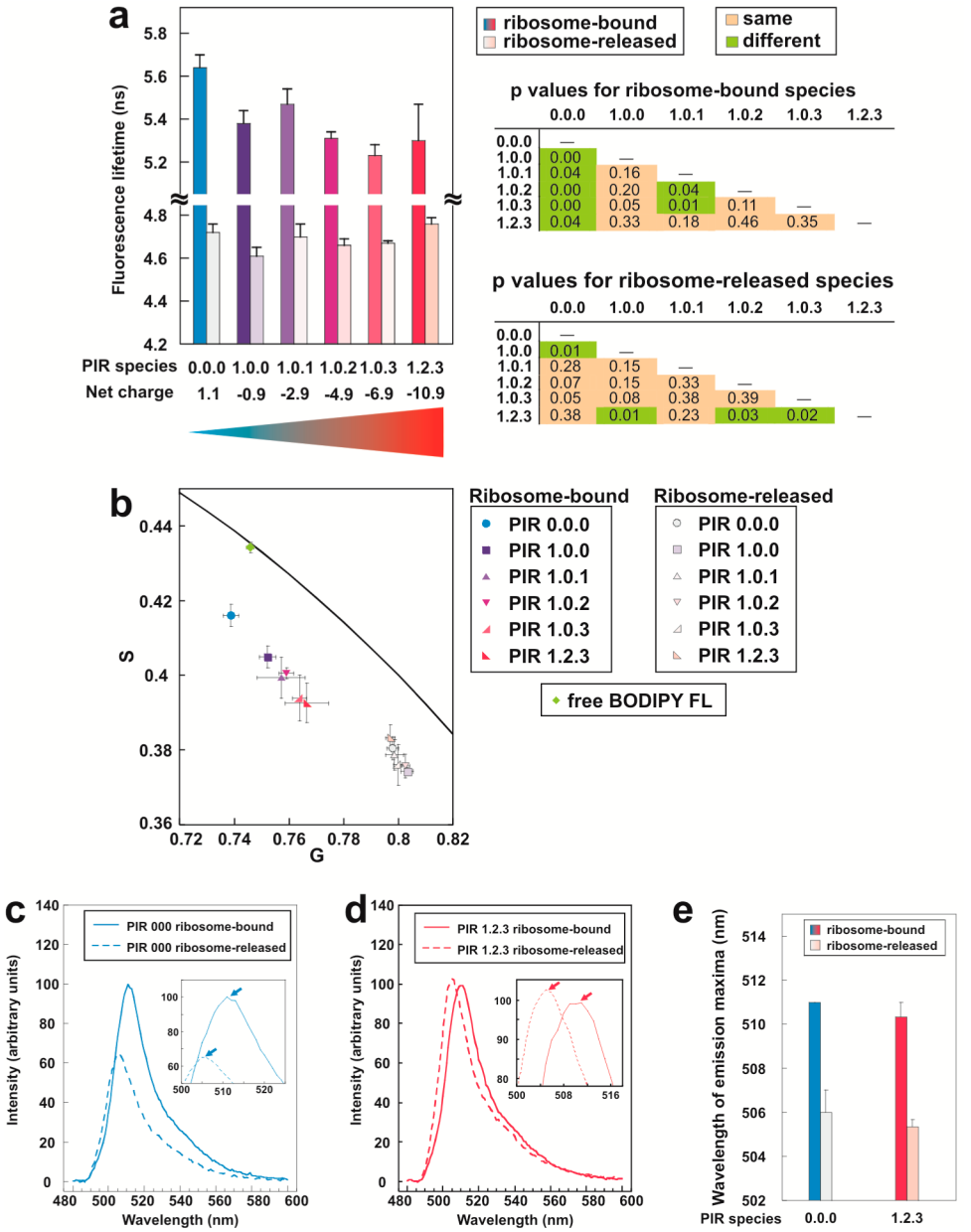

Figure 3. Fluorescence lifetime and intensity of ribosome-bound and -released wild-type and negatively charged PIR variants. (a) Average fluorescence lifetime of ribosome-bound and -released PIR. Error bars denote ± SEM for n = 3−18. The p-value table shows the results from the one-tailed Student's test assuming unequal variances (Welch's t test). Green highlights denote pairs of values that are different with ≥95% confidence. (b) Phasor plot of PIR ribosome-bound, ribosome-released lifetime data and free Bodipy fluorophore, at 16.5 MHz modulation frequency. (c) Emission spectra of ribosome-bound and ribosome-released $PIR_{0.0.0}$ and (d) $PIR_{1.2.3}$ upon excitation at 473 nm. The arrows in the inset highlight the shift in fluorescence emission maximum upon ribosome release. (e) Block diagram illustrating the maxima of the emission spectra of ribosome-bound and ribosome-released $PIR_{0.0.0}$ and $PIR_{1.2.3}$. Error bars show standard errors for three independent experiments.

while the second population has an N terminus that undergoes completely isotropic rotational motions, though it is still 100% ribosome-bound as independently assessed by SDS-PAGE. The two populations may well be in dynamic exchange on a time scale much slower than the excited state decay (i.e., > ns). Assessment of actual mutual interconversion exchange rates, on the other hand, requires different experiments and is beyond the scope of this work.

While more than 90% of wild-type PIR experiences highly biased motions, the data display a distinct trend as a function of the nascent protein's net charge. The apparent fraction of the spatially biased species decreases as the PIR nascent chain becomes more negatively charged (Figure 4b and c). Hence, a greater net negative charge of the nascent chain leads to an increased percentage of the highly dynamic species. While our data do not provide explicit evidence for interactions with the ribosome, it is likely that the biased motions result from interactions of the positively and weakly negatively charged PIR nascent chains with the negatively charged ribosomal surface. Interestingly, the most negatively charged PIR variant, $PIR_{1.2.3}$, still displays about 58% of the spatially biased population. This result highlights the fact that the large electrostatic repulsion between negatively charged nascent chains and the ribosomal surface must be complemented by additional forces, possibly of

dx.doi.org/10.1021/cb400030n | ACS Chem. Biol. 2013, 8, 1195−1204

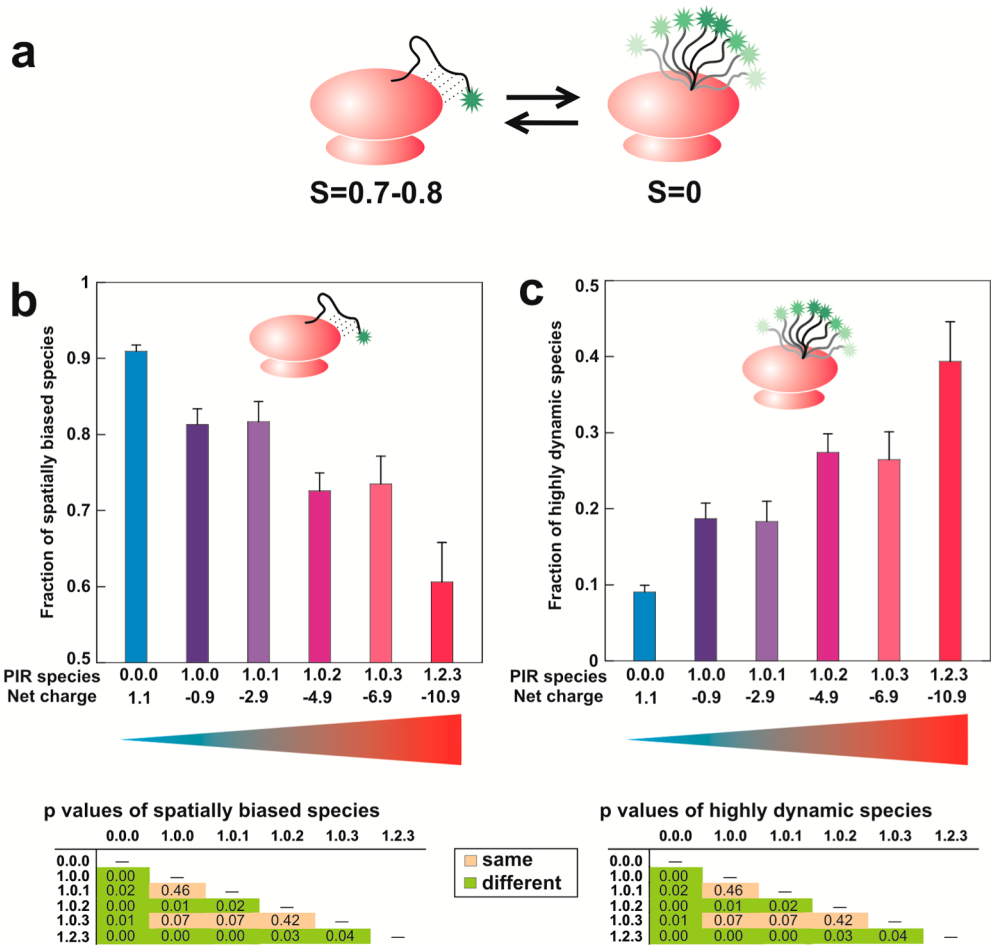

Figure 4. Two RNC populations with different dynamic behavior identified via dynamic fluorescence depolarization. (a) Cartoon representing the two populations. One species has biased dynamics and senses the ribosomal motion, while the other species is highly dynamic with isotropic local motions. (b) Apparent fraction of spatially biased species for the PIR variants examined. (c) Apparent fraction of the highly dynamic species for the PIR variants. Error bars denote ± SEM for n = 3−18. The p values from Student's t test for the data plotted in panels b and c are tabulated, with green indicating that the two values are different with ≥95% confidence.

non-electrostatic nature, responsible for partially biasing the nascent protein motions even in the presence of large electrostatic repulsive components.

As mentioned above, the motions of the N-terminal region of the highly dynamic RNC fraction encompass the widest possible cone semi-angle (Figure 1g), i.e., 180°. The unusually large amplitude of these motions exceeds by far that of ribosome-released PIR, an intrinsically disordered species (see cone semi-angles in Supplementary Tables 2 and 3). However, chemically denatured ribosome-released PIR (in the presence of 6 M urea, see Supplementary Table 3) behaves similarly to the highly dynamic RNC population in that it has completely isotropic N-terminal local motions. This result suggests that the ribosomal surface acts as a local denaturant for nascent proteins, yet it does so under physiologically relevant conditions.

The spatially biased RNC population has a much less dynamic N-terminus and the cone semi-angle is only about 30° for wild-type $PIR_{0.0.0}$. This angle widens slightly as the nascent chain acquires a more negative character, up to $PIR_{1.0.3}$ (Figure 5a). On the other hand, the most negatively charged nascent chain, $PIR_{1.2.3}$, has a cone semi-angle similar to that of the wild-type $PIR_{0.0.0}$, for reasons, possibly related to charge position and distribution, that are hard to rationalize at this juncture. The data can also be represented in terms of the model-free order parameter S (Figure 5b).

Analysis of weakly positively charged nascent chains that bear only one mutation at different sites (Figure 6a) enables assessing the role played by charge position. Positive-to-negative charge mutations are sensed primarily in proximity of the N-terminus (see $PIR_{1.0.0}$), which bears the fluorescent probe, and not at more remote positions along the chain (e.g., see $PIR_{0.0.1}$, Figure 6b and d, and Supplementary Figure 3).

Dynamics of Ribosome-Released Nascent Chains. Unlike the case of RNCs, the anisotropy data for the ribosome-released species fit best to a simple bi-exponential non-associative decay (Figure 5a and b and Supplementary Table 3). Interestingly, despite the dramatically different net charges of all of the species analyzed, there are no considerable differences in the anisotropy parameters of all of the released proteins. This result reinforces the major conclusion of our work, namely, that the ribosome is responsible for modulating the motions of nascent proteins depending on their net charge.

Effect of Increased Ionic Strength. In the above-discussed experiments, the net ionic strength (not including the ribosomes) is ca. 105 mM, i.e., not too dissimilar from the physiologically relevant ionic strength of a living cell under regular growth conditions.[36,37] To test whether ionic strength

dx.doi.org/10.1021/cb400030n | ACS Chem. Biol. 2013, 8, 1195−1204

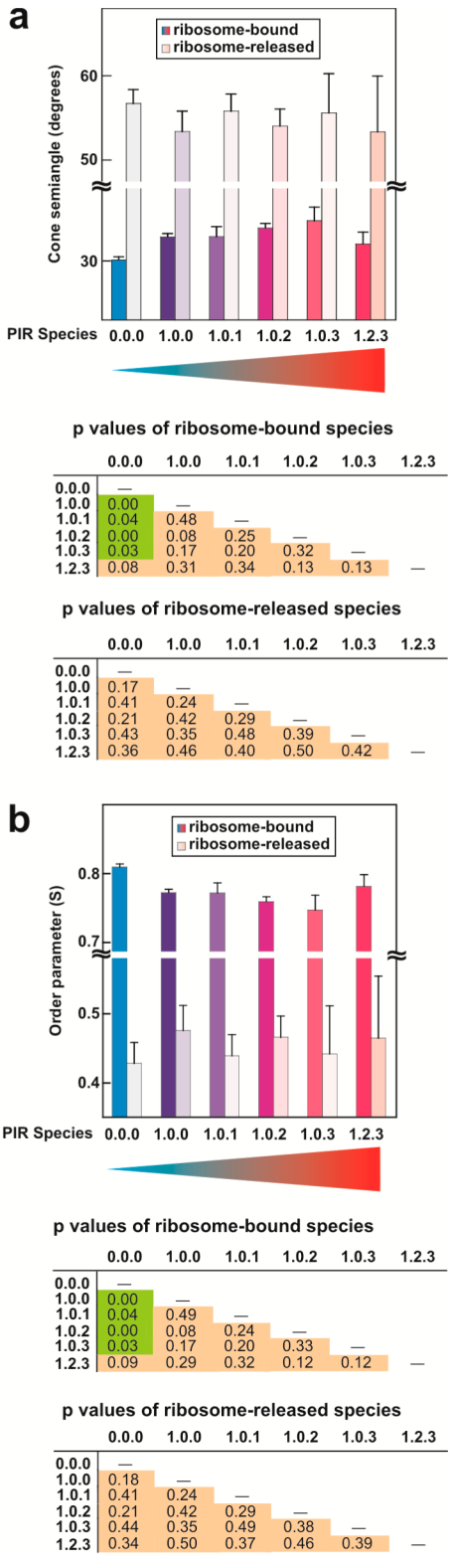

Figure 5. Local dynamics of the spatially biased nascent PIR and the corresponding ribosome-released chains. (a) Cone semi-angles and (b) order parameters are shown. Error bars denote ± SEM for n = 3–18. The p values from the Student's t test are tabulated, with the green-highlighted digits indicating that the two relevant values are different with ≥95% confidence.

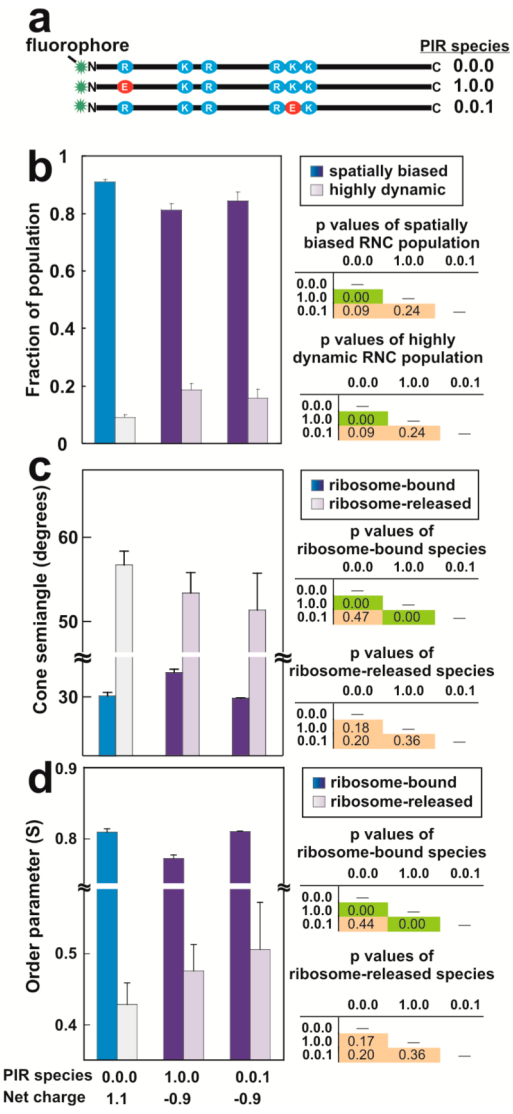

Figure 6. Position-dependence of charges along the PIR nascent chain and its effect on nascent protein dynamics. (a) Schematic diagram of wild-type PIR and PIR variants with a single additional negative charge introduced at two different locations along the chain. (b) Cone semi-angle and (c) order parameters for the spatially biased RNC populations (expressed as apparent fractions) and ribosome-released chains. Error bars denote ± SEM for n = 3–18. The p values from the Student's t test are tabulated, with the green-highlighted digits indicating that the two relevant values are different with ≥95% confidence.

plays any role in RNC dynamics, we increased the amount of salt in the medium by adding 500 mM NaCl to the RNC resuspension buffer. The resulting ionic strength does not alter the ribosome's integrity, as it is compatible with fully assembled ribosomes.[38] We found that, by all criteria examined in this work, namely, fluorescence lifetime, fraction of dynamic and biased species, and amplitude of the motions of the biased species, the increased ionic strength has essentially no effect on the properties of ribosome-bound nascent PIR (Supplementary Figure 4). This conclusion applies to both $PIR_{0.0.0}$ and $PIR_{1.2.3}$, and hence it does not depend on the net charge of the nascent protein. These data can be explained upon considering that there is an increased concentration of positively charged counterions in proximity of the surface of nucleic acids, including DNA[39,40] and predominantly RNA-based species like the ribosome.[27] This effect may take place to a similar extent at

dx.doi.org/10.1021/cb400030n | ACS Chem. Biol. 2013, 8, 1195–1204

low and high ionic strength, until neutralization of the negative potential of the ribosome has been achieved. If this scenario applies, no significant variations in Debye length[41] or nascent chain properties are expected at higher-than-physiological ionic strength.

Interestingly, while high ionic strength does not modify RNC properties, it has a small effect on the features of the ribosome-released protein (Supplementary Figure 4c and d). The only statistically significant effect is on wild-type ribosome-released PIR, where the increased ionic strength decreases the amplitude of the motions of the N-terminus, probably due to an increased degree of charge shielding.

Working Model for RNC Dynamics and Conclusions. In summary, the data discussed so far (Figures 3−6 and Supplementary Tables 1−3) support the simple schematic view of Figure 7a−c. According to this model, the nascent chains of the intrinsically disordered protein PIR, devoid of any bound molecular chaperones,[5,22] interact significantly with the ribosomal surface. This effect is maximized in the case of the positively charged wild-type $PIR_{0.0.0}$, which predominantly comprises a highly spatially biased population (Figure 7a). The fact that significant biases are also present for highly negatively charged RNCs (Figure 7b) is unexpected and may be due to interactions between RNCs and positively charged ribosomal proteins. The tendency of nascent proteins to be significantly dynamically biased regardless of their net charge has biological implications for *in vivo* protein biogenesis. The highly dynamically biased population is likely protected from cotranslational aggregation, premature degradation, and interaction with undesired biomolecules before completion of biosynthesis and folding.

As the net negative charge of the nascent protein increases, a larger population of the highly dynamic nascent chain is generated. This species is extremely flexible and it has completely isotropic N-terminal local motions, much like ribosome-released PIR in 6 M urea (Figure 7c), and similarly or more than other *in vitro* chemically denatured pure proteins analyzed via frequency-domain anisotropy decay spectroscopy.[42,43] Remarkably, this species is populated under physiologically relevant conditions, in the absence of denaturing agents, due to the mere action of the ribosomal surface. We propose that the role of this highly flexible population is to ensure the widest conformational space sampling, and minimize the possibility of cotranslational kinetic trapping. Interestingly, a small population of highly dynamic RNCs exists even for the positively charged wild-type nascent PIR, suggesting that some degree of dynamics is important for all nascent proteins, regardless of their net charge, to ensure proper folding and/or release from the ribosome.

As shown in Figure 7d, the distribution of net charge for all nascent *E. coli* proteins emerging out of the ribosomal tunnel is bimodal. Hence, nascent proteins are either negatively (isoelectric point, pI < 7.4) or positively (pI > 7.4) charged under physiological conditions and rarely bear no net charge. The same concept applies to the distribution of net charge of the corresponding full-length proteins (Supplementary Figure S8). We showed here that nascent proteins differing in the sign and magnitude of their net charge bear a different fraction of highly dynamic and spatially biased species and likely interact with the ribosome to a different degree. A direct implication is that positively charged proteins, which interact more with the ribosome, are more prone to be protected from undesirable events including cotranslational aggregation. This may be an

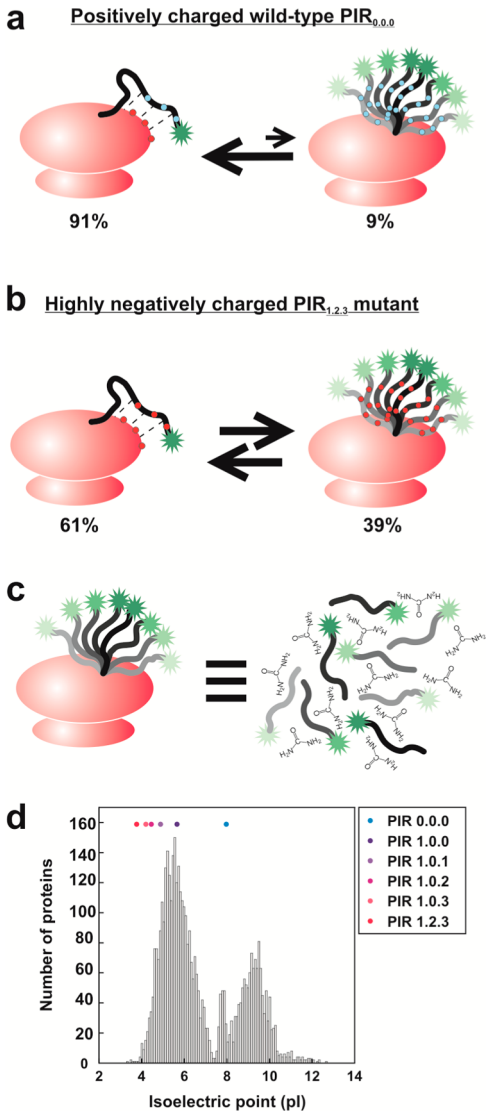

Figure 7. Cartoon illustrating the proposed model for the observed dynamics of (a) wild-type and (b) highly negatively charged PIR. The population of the highly dynamic species increases significantly upon introduction of negatively charged side chain mutations to the PIR chain. (c) Image showing that proximity to the ribosomal surface renders a fraction of the PIR nascent chain as flexible as urea-denatured ribosome-released PIR. (d) Isoelectric point (pI) distribution of C-terminally truncated nascent chains in the *E.coli* K12 proteome. Full-length protein sequences were obtained from SwissProt.[52] The expected pI of the corresponding truncated proteins was then generated upon removal of the last 30 C-terminal residues from each sequence, to eliminate contributions from residues buried within the ribosomal tunnel. Nascent chains shorter than five residues were omitted from the analysis. A Python script was employed to compute all pI values via the Biopython module.[53] PIR and its mutants are displayed above the distribution plot according to their respective pI values.

important feature of ribosomes that evolved early in time, given that bimodal pI distributions have consistently been found across the proteomes of bacteria and archaea.[44,45] Proteomes from eukarya are more complex,[44,45] and so are their matching ribosomes.[46]

Importantly, the range of nascent-chain pI values analyzed in this study is representative of all proteins across the bacterial proteome, as illustrated in Figure 7d, with the exception of

dx.doi.org/10.1021/cb400030n | *ACS Chem. Biol.* 2013, 8, 1195−1204

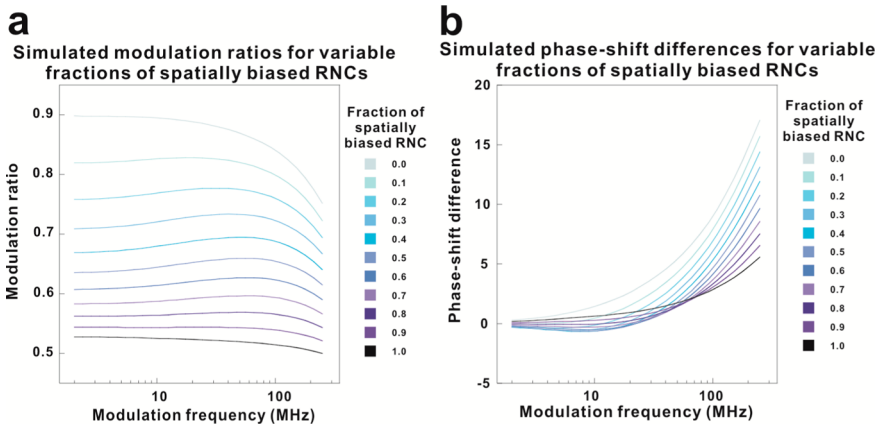

Figure 8. Computer simulations illustrating expected dynamic fluorescence depolarization (a) modulation ratios and (b) phase-shift differences in the presence of two distinct species with different motional characteristics (according to the associative model of Supplementary Figure 3). The representative lifetimes and anisotropy parameters employed in the simulations are the experimentally detected parameters for ribosome-bound $PIR_{1.2.3}$ (see Supplementary Tables 1 and 2), except for the relative fractions of spatially biased and highly dynamic species, which were varied as part of the simulation. The limiting cases, with fraction of spatially biased RNCs set to either 0.0 or 1.0, illustrate the expected spectral profiles for a non-associative model. It is evident that these limiting cases lack the raise in modulation ratio at high frequency and the negative phase-shift differences detected in our experimental data for PIR RNCs. Hence, the results of the simulations support the presence of two types of populations in wild-type and mutant PIR RNCs. The simulations were carried out with the Globals software suite (LFD).

high-p*I* proteins, which are expected to interact with the ribosome even more than wild-type PIR (note that this species is already predominantly ribosome-associated). In the case of non-IDP sequences, the greater fraction of nonpolar residues may introduce additional features (e.g., tendency to undergo intramolecular hydrophobic collapse, affinity for molecular chaperones) that are not addressed in this work.

In conclusion, this study shows that the net charge of a ribosome-bound nascent protein has a dramatic effect on its local dynamics. This effect is likely dominated by electrostatic interactions between the nascent protein and the ribosomal surface. The significant population of dynamically biased RNCs that is found even in the case of highly negatively charged PIR suggests that the nascent protein preserves a high degree of "sticking" even in the absence of a highly attractive potential. The ribosomal surface causes a portion of the nearby nascent chain to be highly flexible, thus acting locally as an effective denaturing agent under physiologically relevant conditions.

METHODS

Definition of PIR and Its Mutants. Wild-type and mutant PIR were denoted according to the number of mutations in each of three regions bearing positively charged residues (Figure 1), as follows. PIR 0.0.0: no mutations; PIR 1.0.0: R6E; PIR 1.0.1: R6E, K45E; PIR 1.0.2: R6E, K45E, K46E; PIR 1.0.3: R6E, R44E, K45E, K46E; PIR 1.2.3: R6E, K22E, R24E, R44E, K45E, K46E.

Generation of RNCs and Ribosome-Released Proteins. Details on the procedures employed to generate RNCs and ribosome-released chains are provided in the Supporting Information.

Fluorescence Anisotropy Decay Data Collection and Analysis. Fluorescence lifetime and anisotropy-decay data were collected via the multifrequency phase and modulation approach on a Chronos spectrofluorometer (ISS) following previously established procedures.[22] The fluorometer was equipped with calcite prism polarizers and a laser diode with λ_{ex} = 473 nm. Fluorescence emission was detected through a 515 nm high-pass filter (51294, Oriel Instr.-Newport Corp.). Data were collected at 25 °C, and samples were equilibrated for at least 20 min at 25 °C before data collection. Lifetime measurements were carried out with a vertically oriented polarizer on the excitation channel and a polarizer oriented at 54.7° on the emission channel. Anisotropy decay data, including all phase-difference and modulation-ratio traces, were corrected with polynomials derived from independently determined frequency-dependent G-factors. The Vinci software suite (ISS) was used to record all collected data and, together with Excel (Microsoft), for implementing the G-factor correction. Analysis and curve fitting of lifetime and polarization data were carried out with the Globals software suite (LFD). Frequency-independent instrumental errors of 0.2° and 0.004 were used for phase and modulation, respectively, in the χ^2 calculations accompanying curve fitting. All lifetime data required fitting to multi-exponential decay expressions including three discrete components: two accounting for the lifetimes of the fluorophore and one additional component (with fictitious lifetime fixed at τ_{Sc} = 1 ps) accounting for very small amounts of light scattering. The scattering component comprised less than 1% of the total detected fluorescence intensity. The fluorescence depolarization data of the ribosome-released samples were fit to two exponentially decaying components. The fundamental anisotropy $r(0)$ was fixed at 0.37, and both fractional amplitudes and rotational correlation times were allowed to vary during the fit. The ribosome-bound samples required fitting to an associative model due to (a) the characteristic rise in modulation ratio at high modulation frequencies and the slightly negative phase differences[33,34] and (b) the lower reduced χ^2 than non-associative multi-exponential decay fits (Supplementary Figure 6). The simplest associative model adequately fitting the data comprises two independently tumbling populations, each associated with one of the fluorophore lifetimes (Supplementary Figure 2). Representative spectral simulations illustrate the expected rise in modulation ratio at high frequencies and the negative phase difference in the presence of two populations with differing motional features (Figure 8). These spectral features require data fitting according to an associative model.[33,34] See the Supporting Information for more details on the associative model and corresponding data fitting procedures.

The amplitude of the N-terminal motions of PIR and its variants were determined by (a) computing order parameters according to the model-free approach by Lipari and Szabo[47] and (b) determining cone semi-angles assuming diffusive motions across a cone,[48] following known procedures.[5]

Steady-State Fluorescence Data Collection. Steady-state fluorescence spectra were acquired at 25 °C on a PC1 fluorimeter (ISS) equipped with a 495 nm long-pass filter (HHQ495lp, Chroma) on the emission channel. The slit widths were set to 0.5 mm (corresponding to a 4 nm bandwidth) on both the excitation and emission channels. The excitation wavelength was 473 nm. Samples

were pre-equilibrated for at least 20 min at 25 °C prior to data collection.

Modeling of the Ribosomal Surface and Electrostatic Calculations. We performed electrostatic surface potential calculations on both the *T. thermophilus* [49] (PDB: 2X9S) and *E. coli* [50] (PDB: 2AVY and 2AW4) 70S ribosomes (Figure 1b and Supplementary Figure 7) with the APBS software package.[51] Additional details are provided in the Supporting Information.

■ ASSOCIATED CONTENT

Supporting Information

Additional information on experimental and computational procedures; details on fluorescence anisotropy decay theory; lifetime and anisotropy decay data tables; supporting figures on control experiments, charge-position dependence, variable salt concentration, gel analysis, additional surface potential maps, and p*I* distribution plots. This material is available free of charge via the Internet at http://pubs.acs.org.

■ AUTHOR INFORMATION

Corresponding Author

*E-mail: cavagnero@chem.wisc.edu.

Present Addresses

[‖]Department of Biology, Massachusetts Institute of Technology, 77 Massachusetts Avenue, Boston, MA 02139.

[⊥]Department of Biochemistry and Molecular Pharmacology, University of Massachusetts Medical School, 364 Plantation Street, Worcester, MA 01605.

Author Contributions

[§]These authors contributed equally to this work.

Notes

The authors declare no competing financial interest.

■ ACKNOWLEDGMENTS

We thank E. Gratton, D. Jameson, the late R. Clegg, and T. Record for enlightening discussions. We are grateful to D. Livermore for technical assistance and to R. Clausen for sharing a Python script. This research was supported by NSF grant MCB-0951209 (to S.C.). P.H.C. and A.M.K. are recipients of UW Madison Hilldale Research Awards in 2009 and 2012, respectively.

■ ABBREVIATIONS

PIR, phosphorylated insulin receptor interaction region of Grb14; IDP, intrinsically disordered protein; RNC, ribosome-bound nascent chain

■ REFERENCES

(1) Cabrita, L. D., Dobson, C. M., and Christodoulou, J. (2010) Protein folding on the ribosome. *Curr. Opin. Struct. Biol. 20*, 33−45.

(2) Clark, P. L., and Ugrinov, K. G. (2009) Measuring Cotranslational Folding of Nascent Polypeptide Chains on Ribosomes, in *Methods in Enzymology*, pp 567−590, Elsevier Academic Press Inc., San Diego.

(3) Fedyukina, D. V., and Cavagnero, S. (2011) Protein folding at the exit tunnel. *Annu. Rev. Biophys. 40*, 337−359.

(4) Gershenson, A., and Gierasch, L. M. (2011) Protein folding in the cell: challenges and progress. *Curr. Opin. Struct. Biol. 21*, 32−41.

(5) Ellis, J. P., Culviner, P. H., and Cavagnero, S. (2009) Confined dynamics of a ribosome-bound nascent globin: Cone angle analysis of fluorescence depolarization decays in the presence of two local motions. *Protein Sci. 18*, 2003−2015.

(6) Wilson, D. N., and Beckmann, R. (2011) The ribosomal tunnel as a functional environment for nascent polypeptide folding and translational stalling. *Curr. Opin. Struct. Biol. 21*, 274−282.

(7) Woolhead, C. A., McCormick, P. J., and Johnson, A. E. (2004) Nascent membrane and secretory proteins differ in FRET-detected folding far inside the ribosome and in their exposure to ribosomal proteins. *Cell 116*, 725−736.

(8) Tu, L. W., and Deutsch, C. (2010) A folding zone in the ribosomal exit tunnel for Kv1.3 helix formation. *J. Mol. Biol. 396*, 1346−1360.

(9) Ban, N., Nissen, P., Hansen, J., Moore, P. B., and Steitz, T. A. (2000) The complete atomic structure of the large ribosomal subunit at 2.4 angstrom resolution. *Science 289*, 905−920.

(10) Trylska, J., Konecny, R., Tama, F., Brooks, C. L., and McCammon, J. A. (2004) Ribosome motions modulate electrostatic properties. *Biopolymers 74*, 423−431.

(11) Kaiser, C. M., Goldman, D. H., Chodera, J. D., Tinoco, I., and Bustamante, C. (2011) The ribosome modulates nascent protein folding. *Science 334*, 1723−1727.

(12) O'Brien, E. P., Christodoulou, J., Vendruscolo, M., and Dobson, C. M. (2011) New scenarios of protein folding can occur on the ribosome. *J. Am. Chem. Soc. 133*, 513−526.

(13) Dong, F., Olsen, B., and Baker, N. A. (2008) Computational methods for biomolecular electrostatics, in *Biophysical Tools for Biologists*, Vol. *1*, In Vitro Techniques, pp 843−870, Elsevier Academic Press Inc, San Diego.

(14) Gitlin, I., Carbeck, J. D., and Whitesides, G. M. (2006) Why are proteins charged? Networks of charge-charge interactions in proteins measured by charge ladders and capillary electrophoresis. *Angew. Chem., Int. Ed. 45*, 3022−3060.

(15) Sharp, K. A., and Honig, B. (1990) Electrostatic interactions in macromolecules - theory and applications. *Annu. Rev. Biophys. Biophys. Chem. 19*, 301−332.

(16) Dill, K. A. (1990) Dominant Forces in Protein Folding. *Biochemistry (Moscow) 29*, 7133−7155.

(17) Zbilut, J. P., Giuliani, A., Colosimo, A., Mitchell, J. C., Colafranceschi, M., Marwan, N., Webber, C. L., and Uversky, V. N. (2004) Charge and hydrophobicity patterning along the sequence predicts the folding mechanism and aggregation of proteins: A computational approach. *J. Proteome Res. 3*, 1243−1253.

(18) Uversky, V. N., Gillespie, J. R., and Fink, A. L. (2000) Why are "natively unfolded" proteins unstructured under physiologic conditions? *Proteins: Struct., Funct., Genet. 41*, 415−427.

(19) Mao, A. H., Crick, S. L., Vitalis, A., Chicoine, C. L., and Pappu, R. V. (2010) Net charge per residue modulates conformational ensembles of intrinsically disordered proteins. *Proc. Natl. Acad. Sci. U.S.A. 107*, 8183−8188.

(20) Moncoq, K., Broutin, I., Larue, V., Perdereau, D., Cailliau, K., Browaeys-Poly, E., Burnol, A. F., and Ducruix, A. (2003) The PIR domain of Grb14 is an intrinsically unstructured protein: implication in insulin signaling. *FEBS Lett. 554*, 240−246.

(21) Moncoq, K., Broutin, I., Craescu, C. T., Vachette, P., Ducruix, A., and Durand, D. (2004) SAXS study of the PIR domain from the Grb14 molecular adaptor: A natively unfolded protein with a transient structure primer? *Biophys. J. 87*, 4056−4064.

(22) Ellis, J. P., Bakke, C. K., Kirkdoerfer, R. N., Jungbauer, L. M., and Cavagnero, S. (2008) Chain dynamics of nascent polypeptides emerging from the ribosome. *ACS Chem. Biol. 3*, 557−566.

(23) Malkin, L. I., and Rich, A. (1967) Partial resistance of nascent polypeptide chains to proteolytic digestion due to ribosomal shielding. *J. Mol. Biol. 26*, 329−347.

(24) Voss, N. R., Gerstein, M., Steitz, T. A., and Moore, P. B. (2006) The geometry of the ribosomal polypeptide exit tunnel. *J. Mol. Biol. 360*, 893−906.

(25) Weinreis, S. A., Ellis, J. P., and Cavagnero, S. (2010) Dynamic fluorescence depolarization: A powerful tool to explore protein folding on the ribosome. *Methods 52*, 57−73.

(26) Kinosita, K., Jr., Ikegami, A., and Kawato, S. (1982) On the wobbling-in-cone analysis of fluorescence anisotropy decay. *Biophys. J. 37*, 461−4.
(27) Guttman, H. J., Cayley, S., Li, M., Anderson, C. F., and Record, M. T. (1995) K+ ribosome interactions determine the large enhancements of K-39 NMR transverse relaxation rates in the cytoplasm of Escherichia coli K-12. *Biochemistry (Moscow) 34*, 1393−1404.
(28) Redford, G. I., and Clegg, R. M. (2005) Polar plot representation for frequency-domain analysis of fluorescence lifetimes. *J. Fluoresc. 15*, 805−815.
(29) Stefl, M., James, N. G., Ross, J. A., and Jameson, D. M. (2011) Applications of phasors to in vitro time-resolved fluorescence measurements. *Anal. Biochem. 410*, 62−69.
(30) Jameson, D. M., Gratton, E., and Hall, R. D. (1984) The measurement and analysis of heterogeneous emissions by multi-frequency phase and modulation fluorometry. *Appl. Spectrosc. Rev. 20*, 55−106.
(31) Buscaglia, R., Jameson, D. M., and Chaires, J. B. (2012) G-quadruplex structure and stability illuminated by 2-aminopurine phasor plots. *Nucleic Acids Res. 40*, 4203−4215.
(32) Lakowicz, J. R. (2006) *Principles of Fluorescence Spectroscopy*, Kluwer Academic/Plenum Publishing, New York.
(33) Szmacinski, H., Jayaweera, R., Cherek, H., and Lakowicz, J. R. (1987) Demonstration of an associated anisotropy decay by frequency-domain fluorometry. *Biophys. Chem. 27*, 233−241.
(34) Hazlett, T. L., and Jameson, D. L. (1988) Time-resolved fluorescence studies on components of the prokaryotic protein elongation system. *Proc. SPIE 909*, 412−419.
(35) Bialik, C. N., Wolf, B., Rachofsky, E. L., Ross, J. B. A., and Laws, W. R. (1998) Dynamics of biomolecules: Assignment of local motions by fluorescence anisotropy decay. *Biophys. J. 75*, 2564−2573.
(36) Record, M. T., Courtenay, E. S., Cayley, S., and Guttman, H. J. (1998) Biophysical compensation mechanisms buffering E. coli protein-nucleic acid interactions against changing environments. *Trends Biochem. Sci. 23*, 190−194.
(37) Record, M. T., Courtenay, E. S., Cayley, D. S., and Guttman, H. J. (1998) Responses of E. coli to osmotic stress: Large changes in amounts of cytoplasmic solutes and water. *Trends Biochem. Sci. 23*, 143−148.
(38) Jelenc, P. C. (1980) Rapid purification of highly-active ribosomes from Escherichia coli. *Anal. Biochem. 105*, 369−374.
(39) Anderson, C. F., and Record, M. T. (1995) Salt nucleic-acid interactions. *Annu. Rev. Phys. Chem. 46*, 657−700.
(40) Anderson, C. F., and Record, M. T. (1982) Poly-electrolyte theories and their applications to DNA. *Annu. Rev. Phys. Chem. 33*, 191−222.
(41) Rubinstein, M., and Colby, R. H. (2003) *Polymer Physics*, Oxford University Press, New York.
(42) Thevenin, B. J. M., Periasamy, N., Shohet, S. B., and Verkman, A. S. (1994) Segmental dynamics of the cytoplasmic domain of erythrocyte band-3 determined by time-resolved fluorescence anisotropy - sensitivity to pH and ligand-binding. *Proc. Natl. Acad. Sci. U.S.A. 91*, 1741−1745.
(43) Mei, G., Rosato, N., Silva, N., Rusch, R., Gratton, E., Savini, I., and Finazziagro, A. (1992) Denaturation of human Cu/Zn superoxide-dismutase by guanidine-hydrochloride - a dynamic fluorescence study. *Biochemistry (Moscow) 31*, 7224−7230.
(44) Kiraga, J., Mackiewicz, P., Mackiewicz, D., Kowalczuk, M., Biecek, P., Polak, N., Smolarczyk, K., Dudek, M. R., and Cebrat, S. (2007) The relationships between the isoelectric point and: length of proteins, taxonomy and ecology of organisms. *BMC Genomics 8*, 163.
(45) Schwartz, R., Ting, C. S., and King, J. (2001) Whole proteome pI values correlate with subcellular localizations of proteins for organisms within the three domains of life. *Genome Res. 11*, 703−709.
(46) Wilson, D. N., and Cate, J. H. D. (2012) The Structure and Function of the Eukaryotic Ribosome. *Cold Spring Harb. Perspect. Biol. 4*, No. a011536.
(47) Lipari, G., and Szabo, A. (1980) Effect of librational motion on fluorescence depolarization and nuclear magnetic resonance relaxation in macromolecules and membranes. *Biophys. J. 30*, 489−506.
(48) Kinosita, K., Jr., Ikegami, A., and Kawato, S. (1982) On the wobbling-in-cone analysis of fluorescence anisotropy decay. *Biophys. J. 37*, 461−4.
(49) Jin, H., Kelley, A. C., Loakes, D., and Ramakrishnan, V. (2010) Structure of the 70S ribosome bound to release factor 2 and a substrate analog provides insights into catalysis of peptide release. *Proc. Natl. Acad. Sci. U.S.A. 107*, 8593−8598.
(50) Schuwirth, B. S., Borovinskaya, M. A., Hau, C. W., Zhang, W., Vila-Sanjurjo, A., Holton, J. M., and Cate, J. H. D. (2005) Structures of the bacterial ribosome at 3.5 Ångstrom resolutio. *Science 310*, 827−834.
(51) Baker, N. A., Sept, D., Joseph, S., Holst, M. J., and McCammon, J. A. (2001) Electrostatics of nanosystems: Application to microtubules and the ribosome. *Proc. Natl. Acad. Sci. U.S.A. 98*, 10037−10041.
(52) Bairoch, A., and Apweiler, R. (2000) The SWISS-PROT protein sequence database and its supplement TrEMBL in 2000. *Nucleic Acids Res. 28*, 45−48.
(53) Cock, P. J. A., Antao, T., Chang, J. T., Chapman, B. A., Cox, C. J., Dalke, A., Friedberg, I., Hamelryck, T., Kauff, F., Wilczynski, B., and de Hoon, M. J. L. (2009) Biopython: freely available Python tools for computational molecular biology and bioinformatics. *Bioinformatics 25*, 1422−1423.